JOURNAL OF GEOPHYSICAL RESEARCH, VOL. 104, NO. B10, PAGES 22,845–22,858, OCTOBER 10, 1999

Forces driving ridge propagation

Brian P. West[1] and Jian Lin
Dept. of Geology and Geophysics, Woods Hole Oceanographic Institution, Woods Hole, Massachusetts

David M. Christie
College of Oceanic and Atmospheric Sciences, Oregon State University, Corvallis

Abstract. Recent multibeam bathymetric and geophysical data from the Southeast Indian Ridge (SEIR) reveal eight propagating ridges (PRs) moving down the regional bathymetry gradient toward the Australian-Antarctic Discordance (AAD). These PRs are propagating at a nearly uniform rate of 40- mm yr^{-1} despite dramatic variations in axial morphology and segment length, and local reversals of the regional bathymetric gradient. Because existing dynamic rift propagation models do not explain the continued, uniform propagation of the diverse SEIR PRs, we have developed a new model that includes variable crustal thickness and thermally-driven, along-axis asthenospheric flow, in addition to topographic gradients, as positive contributions to the forces driving rift propagation. Along-axis asthenospheric flow and variations in crustal thickness along the SEIR appear to provide the first-order driving force required for ridge propagation, even in the highly segmented, magmatically starved region in and near the AAD where previous models for ridge propagation fail. Further, our model development requires that the rift valley at the propagating tip is a consequence of rifting in the cooler thermal regime of preexisting lithosphere, rather than a consequence of viscous resistance to flow. This explanation of PR tip topography is consistent with gravity data from the SEIR that suggest that the rift tip and associated pseudofaults are at least partially compensated by crustal thinning.

1. Introduction

Mid-ocean ridge propagation was first identified by *Shih and Molnar* [1975] and *Hey and Vogt* [1977], and since that time, numerous propagating ridges (PRs) have been recognized along the global mid-ocean ridge system. Ridge propagation is one end-member in a continuum of migrating spreading center offset types and is a fundamental mechanism for the development and modification of mid-ocean ridge segmentation. Evidence for the widespread occurrence of PRs can be found in the numerous pseudofaults traces that are evident in global satellite gravity anomaly data [*Phipps Morgan and Sandwell*, 1994] and in more detailed, shipboard studies of ridge axis morphology. To date, propagating rifts have been studied and modeled on the East Pacific Rise (EPR) [*Carbotte et al.*, 1991; *Macdonald and Fox*, 1983; *Macdonald et al.*, 1984; *Perram et al.*, 1993], the Cocos-Nazca spreading center [*Christie and Sinton*, 1986; *Kleinrock and Hey*, 1989a,b; *Kleinrock et al.*, 1989; *Phipps Morgan and Parmentier*, 1985, 1986; *Searle and Hey*, 1983; *Sinton et al.*, 1983], the Juan de Fuca Ridge [*Shoberg et al.*, 1991; *Wilson*, 1990; *Wilson and Hey*, 1995; *Wilson et al.*, 1984], the Reykjanes Ridge [*Phipps Morgan and Kleinrock*, 1991; *Vogt*, 1971, 1974], the southern Mid-Atlantic Ridge (MAR) [*Brozena and White*, 1990], the Pacific-Antarctic Ridge [*Géli et al.*, 1997], and the East Scotia Ridge [*Livermore et al.*, 1997]. All of these regions share the common characteristics of a relatively high magma supply, either due to proximity to a hotspot, to their fast spreading environment, or to "a localized melting anomaly" [*Livermore et al.*, 1997].

Concepts from fracture mechanics were first applied to explain propagating mid-ocean ridge segments by *Pollard and Aydin* [1984]. These ideas were further developed by *Sempéré and Macdonald* [1986] and *Phipps Morgan and Parmentier* [1985] to study the EPR (Easter) and the Galápagos (Cocos-Nazca) spreading systems, respectively. Since these pioneering studies, a significantly larger portion of the global mid-ocean ridge system has been mapped by multibeam echo sounders [*Cochran et al.*, 1997; *Grindlay et al.*, 1996; *Scheirer et al.*, 1997; *Sempéré et al.*, 1997, 1996], and considerable advances have been made in our understanding of the mechanisms that produce ridge crest topography [e.g., *Chen and Morgan*, 1990a,b; *Shaw and Lin*, 1996].

Between the Australian-Antarctic Discordance (AAD), near 126°E, and 90°E, the Southeast Indian Ridge (SEIR) undergoes a transition from EPR-like axial highs to MAR-like axial valleys despite a near-constant, intermediate spreading rate (72-76 mm yr^{-1}, full rate) [*Cochran et al.*, 1997; *Sempéré et al.*, 1997, 1996; *West et al.*, 1994, 1997]. Along this part of the SEIR, eight PRs are actively propagating down the regional bathymetric gradient toward the deep region of the AAD (Figures 1 and 2). Although these eight PRs vary dramatically in both segment length and axial morphology (both axial valley and axial high type propagating segments occur), they are all propagating at a nearly uniform rate of 40-50 mm yr^{-1}. They do not conform to the previously proposed correlation between propagation rate and axial topography [*Wilson and Hey*, 1995]. On a local (single segment) scale, several of the SEIR PRs are actually propagating into areas of decreasing axial depth, where the regional bathymetric gradient is locally reversed (Figure 2). These distinctive characteristics of the

[1]Now at Exxon Production Research Company, Houston, Texas.

Paper number 1999JB900154.
0148-0227/99/1999JB900154$09.00

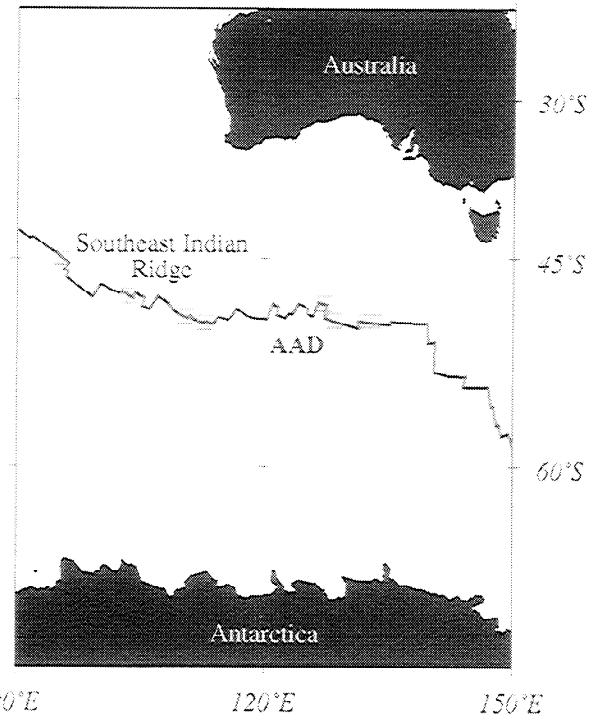

Figure 1. The location of the Southeast Indian Ridge (SEIR) and propagating rift systems of the SEIR analyzed by this study (shaded boxes). The Australian-Antarctic Discordance (AAD) is located between ~115° and ~128°E along the SEIR.

SEIR PRs have prompted us to reexamine the mechanisms of ridge propagation.

We begin our investigation of the SEIR PRs by using the formulation of *Phipps Morgan and Parmentier* [1985] to estimate the driving and resisting forces for ridge propagation along the SEIR, using along-axis variations in seafloor topography. We next extend this model, first to include the contributions of variations in Moho topography to the force driving ridge propagation and then to incorporate regionally driven along-axis asthenospheric flow beneath the SEIR (Figure 2). We demonstrate that this flow can be of first-order significance. Finally, we discuss how this new quantitative model can explain the consistency of ridge propagation, despite the inconsistent morphology and variable topographic gradients along the SEIR.

2. Effects of Seafloor Topography on Ridge Propagation

Numerically, a propagating ridge can be formulated as a crack in an elastic plate (Figure 3) overlying a weak viscous substrate. Within such a framework, *Phipps Morgan and Parmentier* [1985] assumed that the driving forces for ridge propagation are shallow gravitational spreading forces due to excess ridge axis topography relative to off-axis bathymetry. Balancing the ridge-normal force $P(x)$ with the difference in elevation between the on- and off-axis seafloor [*Phipps Morgan and Parmentier*, 1985; *Turcotte and Schubert*, 1982] yields

$$P(x)=(\rho_l-\rho_w)g\delta H/2, \qquad (1)$$

where H is the near-axis elastic plate thickness, g is the acceleration of gravity, δ is the topographic difference between the on- and off-axis seafloor, and ρ_l and ρ_w are the average densities of the lithosphere and water, respectively. This equation was derived from expressions for gravitational sliding associated with ridge push [e.g., *Turcotte and Schubert*, 1982, p. 287]. Implicit in this equation is the assumption that the density contrasts that compensate the ridge axis topography lie between the seafloor (z=0) and a depth of compensation ($\delta+H$) [e.g., *Turcotte and Schubert*, 182, p. 287, Figure 6-43]. Thus (1) can be thought of as an expression for the horizontal force per unit length of ridge axis due to excess topography that is supported by regional Pratt isostasy where the elastic plate (lithospheric) thickness H at the selected off-axis reference location is greater than the crustal thickness. *Phipps Morgan and Parmentier* [1985], for example, assume a reference location ~15 km off-axis with a lithospheric thickness of ~7-8 km. This lithospheric thickness may not be thicker than the crustal thickness in some cases, especially for fast spreading ridges such as the East Pacific Rise or for hotspot-dominated ridges such as the Cocos-Nazca spreading center. This assumption will be modified later.

Treating the propagating ridge as a symmetric, pressurized crack of length $2L$, *Phipps Morgan and Parmentier* [1985] showed that the stress intensity factor at the propagator tip due to excess topography can be calculated as follows (using (1) for $P(x)$):

$$K_I=\frac{2}{H}\left(\frac{L}{\pi}\right)^{1/2}\int_0^L\frac{P(x)dx}{(L^2-x^2)^{(1/2)}} \qquad (2)$$

where K_I is the mode I extensional stress intensity factor for a crack in an elastic plate of thickness H, loaded by a force per unit length $P(x)$ [*Parker*, 1981; *Phipps Morgan and Parmentier*, 1985]. In the first-order approximation of constant H along the ridge axis, employing (1) and (2) requires only a knowledge of the along-axis topographic gradient as H cancels out of the combined equations.

In their study of Galápagos and Easter propagation dynamics, *Phipps Morgan and Parmentier* [1985] assumed that this topographic driving force is counterbalanced by viscous resistance to asthenospheric flow within a subaxial conduit [*Parmentier and Forsyth*, 1985] and that propagation occurs when these two forces are in an appropriate dynamic equilibrium. This is a corollary to the assumption that the depression at propagating tips is dynamically supported by intrasegment along-axis flow [*Parmentier and Forsyth*, 1985]. Because the mass deficit represented by the tip depression supplies a negative contribution to the stress intensity factor, it balances the positive contribution to the stress intensity factor supplied by the topography. These assumptions are not, however, supported by our study of the SEIR propagating ridges (see section 5.2).

3. Ridge Propagation at the SEIR

Eight active PRs have been located along the SEIR between 89° and 145°E, either through direct shipboard observation or through satellite gravity data [*Cochran et al.*, 1997; *Phipps Morgan and Sandwell*, 1994; *Sempéré et al.*, 1997, 1996]. The tips of these PRs are located near 96°, 104°, 111°, 113°, 126° 30', 128°, 131°, and 134°30'E (Figures 1, 4a, and 4b). Complex transitions in axial morphology along some SEIR segments have been described by *Palmer et al.* [1993], *Sempéré*

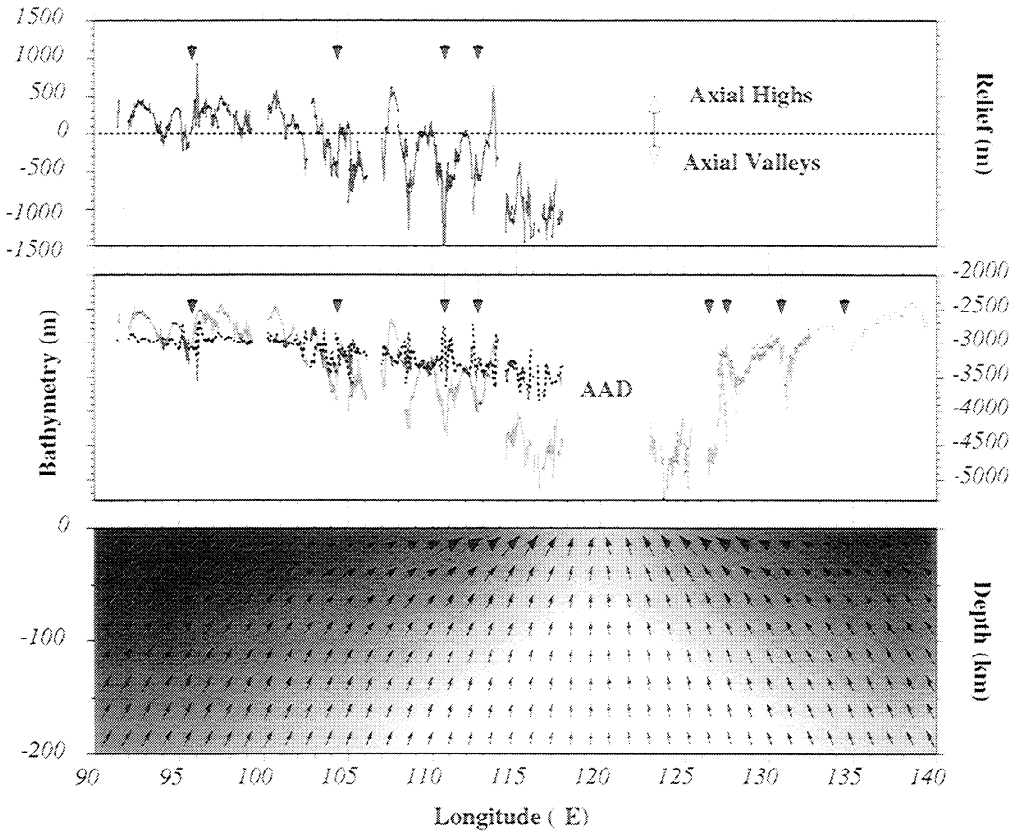

Figure 2. (bottom) Numerical results for a temperature- and pressure-dependent viscosity simulation of buoyant wasthenospheric flow beneath the SEIR with a ~100°C temperature anomaly associated with the AAD [*West et al.*, 1997]. High viscosities beneath the AAD are shown by the lighter shades; the total viscosity variation of these simulations is ~5 orders of magnitude. Vectors show the vertical and axis-parallel components of subaxial mantle flow. The symmetry of these models around 120°E implies that cooler, higher-viscosity upper mantle beneath the AAD will result in significant along-axis flow toward the AAD beneath the SEIR from the east and west, as well as a reduction in mantle upwelling beneath the AAD. These calculations are consistent with the geochemical and geophysical characteristics of the AAD, including the along-axis depth profile shown in the middle panel. (middle) The along-axis depth profile of the SEIR between ~90°E and ~140°E is taken from *West et al.* [1997]. Regionally, the along-axis depth varies by up to 2 km along the length of the SEIR, although locally the axial depths are very "nonmonotonic" [*Sempéré et al.*, 1996; *Shah and Sempéré,* 1998]. The solid dotted line between ~90°E and ~120°E indicates the average off-axis depth. The location of AAD is shown at the center of the regional depression. The approximate locations of the observed PRs are shown by the vertical arrows. (top) The axial bathymetric curve minus the off-axis bathymetric curve of the middle panel. This figure can be thought of as a proxy for the location of axial highs (positive values) and axial valleys (negative values) along the SEIR between ~90°E and ~120°E. Note that many of these PRs are propagating away from an axial valley, and one (113°E) is propagating toward a local bathymetric high, a result unexpected with the simple fracture mechanics model.

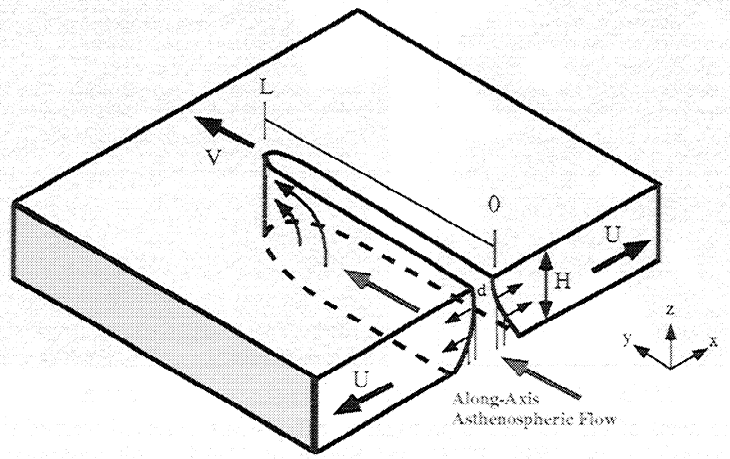

Figure 3. A schematic of the fracture mechanics model of a PR (modified from Figure 2 of *Phipps Morgan and Parmentier* [1985]). See text for summary or *Phipps Morgan and Parmentier* [1985] for full details. Solid line illustrates the along-axis asthenospheric flow caused by the advancing crack tip, and the shaded line indicates regionally driven along-axis asthenospheric flow which we invoke in our flow-driven model.

et al. [1997, 1996], and *Shah and Sempéré* [1998]. The SEIR PRs are located in areas with distinctly different morphologic and segmentation characteristics from the Galápagos and Easter systems. Because of these differences, the SEIR PRs do not appear to conform to previous ridge propagation models that are based heavily on Galápagos and Easter examples. In this paper we examine the specifics of the SEIR PR systems and their implications for more general ridge propagation models.

3.1. Definition of "Excess" Topography in an Axial Valley Setting

Along the Galápagos and Easter PR systems, relatively uninterrupted gradients in axial-high morphology are interpreted to provide the necessary driving force for ridge propagation by increasing the stress intensity factor at the propagator tips [*Phipps Morgan and Parmentier*, 1985]. If this interpretation were directly applied to regions with highly segmented, axial valley ridge morphology, the gravitational contribution to the stress intensity factor (K_I) at the rift tip would be negative, inhibiting rift propagation altogether. This cannot be the case along the SEIR, where short, axial valley segments are propagating at rates equal to or exceeding their spreading rate (Figures 4a and 4b).

A reexamination of the *Phipps Morgan and Parmentier* [1985] model suggests that one possible solution to this dilemma lies in changing the reference level for calculating the 'excess' bathymetry in (1) from a mean off-axis value to the depth of the propagator tip itself. With this modification, even in axial-valley morphology, a positive contribution to the stress intensity factor at the PR tip would result from the shallowness of the propagating segment center relative to its tip. Although this makes the value chosen for K_I sensitive to the choice of the crack tip position, in most cases, the tectonic expression of the propagator tip is well defined in seafloor morphology, and it is relatively easy to reproducibly estimate its geographic position.

3.2. Compensation of Propagating Rift Tips and Pseudofaults

Phipps Morgan and Parmentier [1986] concluded from gravity data that the Galápagos 95.5°W propagating rift tip depression is not compensated by thinned oceanic crust. In contrast, for the SEIR 111°E and 113°E propagators (those for

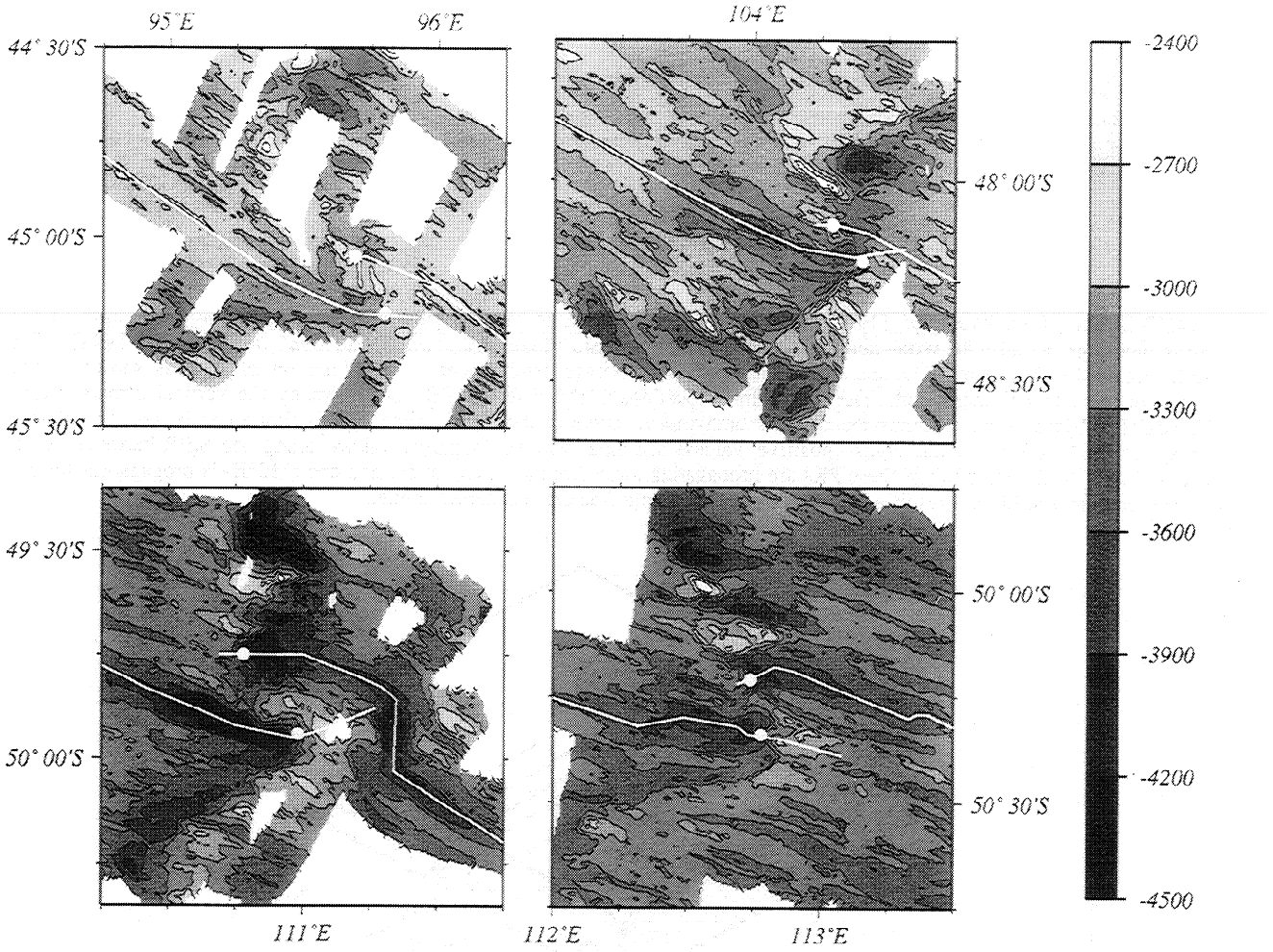

Figure 4a. Bathymetric maps of the four active propagating rift systems observed west of the AAD. Data sources include *Palmer et al.* [1993], *Sempéré et al.* [1996, 1997], and *West et al.* [1994]. All propagators are currently propagating eastward, toward the deepest portions of the AAD. These PRs vary dramatically in their axial morphology and segment length, yet are propagating at a nearly uniform rate of 40-50 mm yr^{-1}. The choice of the crack tip(s) used in our analysis are shown as white dots along the ridge axis (white).

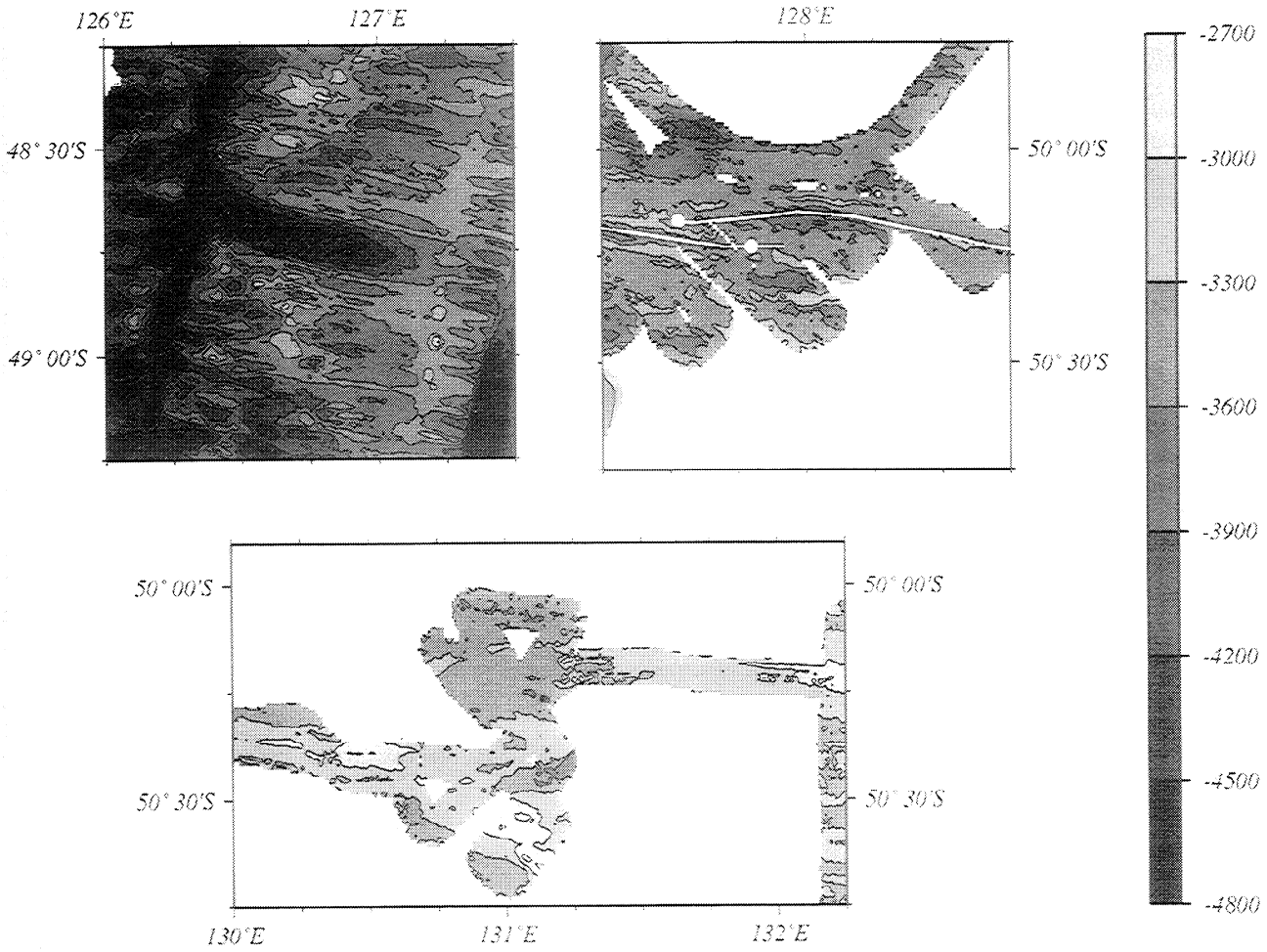

Figure 4b. Bathymetric maps of three of the four active propagating rift systems east of the AAD. All are propagating toward the west. The 134°40' EPR is not shown because there is insufficient multi-beam coverage.

Table 1. PR and FR Characteristics With Driving and Resisting Forces as Defined by *Phipps Morgan and Parmentier* [1985]

Ridge	Longitude, deg	Latitude deg	Depth of Rift Tip. m	Migration Rate, mm yr^{-1}	A, km	B, km	$K_{driving}$, Pa m$^{1/2}$	$K_{resisting}$ Dynamic, Pa m$^{1/2}$	$K_{resisting}$ Isostatic, Pa m$^{1/2}$
96°E PR	95.80	-45.20	-2823	45	62	157	2.5E+08	-5.6E+08	-4.2E+08
104°E PR	104.40	-48.20	-3221	44	0	117	4.6E+08	-1.2E+09	-9.0E+08
111°E PR	110.98	-49.94	-3547	34	55	164	2.7E+08	-1.3E+09	-9.7E+08
113°E PR	112.78	-50.34	-3519	53	50	112	5.8E+07	-7.4E+08	-5.6E+08
128°E PR	127.53	-50.17	-3333	43	50	259	5.1E+08	-7.2E+08	-5.4E+08
96°E FR	95.69	-45.05	-2911	-45	35	66	1.5E+08	-9.8E+07	-7.4E+07
104°E FR	104.29	-48.11	-3307	-44	45	78	1.4E+08	-2.6E+08	-1.9E+08
111°E FR	110.78	-49.75	-3868	-34	60	174	6.4E+08	-5.6E+08	-4.2E+08
113°E FR	112.74	-50.21	-3788	-53	20	92	7.5E+08	-1.3E+08	-1.0E+08
128°E FR	127.80	-50.23	-3554	-43	30	53	7.5E+07	-4.6E+07	-3.5E+07

PR, propagating ridges; FR, failing ridges. Read 2.5E+08 as 2.5×10^8.

which there are sufficient data), distinct positive mantle Bouguer anomalies (MBA) associated with the tip depressions and the pseudofaults (the off-axis traces of the propagating rift tip) suggest that these regions are at least partially compensated by thinner crust (Figure 5, also see *West and Sempéré* [1998]). In Figure 5 the MBA values increase by more than 15 mGal from segment center to PR tip, consistent with crustal thinning of 600-800 m, supporting 150-200 m of compensated topography. Off-axis, along the pseudofaults, MBA increases by 12-16 mGal relative to adjacent regions persist. The persistence of the Bouguer anomaly off axis is consistent with crustal thinning beneath the PR tip,

suggesting, in turn, that the tip depressions result from a combination of relatively thin crust with stretching of a relatively cool lithosphere [*Tapponnier and Francheteau,* 1978; *Chen and Morgan*, 1990a,b; *Neumann and Forsyth*, 1993] and not necessarily from viscous flow within a narrow sub axial conduit.

The possibility that propagating rift tips are underlain by relatively thin crust has significant implications for the balance of propagating and resisting forces that controls propagation. A tip depression that is supported dynamically by viscous flow (as in the work by *Phipps Morgan and Parmentier* [1985]) provides a 33% stronger resistive force than a tip depression that is supported isostatically. Therefore, tip depressions that are produced by a combination of relatively thin crust and lithospheric necking, as appears to be the case for the SEIR, rather than by viscous depression, as proposed for the Easter and Galápagos examples, must involve a significantly different dynamic equilibrium between driving and resisting forces.

3.3. Analysis of the SEIR PRs

Axial topographic profiles for SEIR propagating and failing rifts (FRs) are shown in Figures 6 and 7. For all the PRs, the dynamic forces resisting propagation as defined by *Phipps Morgan and Parmentier* [1985] are greater than the forces driving propagation (Figure 8 and Table 1). Even if the axial valley is assumed to be only 75% supported by Airy isostatic compensation, resisting forces remain larger than driving forces for these PRs (Figure 8 and Table 1). Conversely, for the FRs the calculated driving forces are significantly larger than those resisting propagation (Figure 8 and Table 1) (the only exception is the 104°E FR, which appears to have recently jumped southward from a deep valley to the north; Figure 4a). In other words, this formulation predicts the wrong propagation direction for all SEIR propagating rift systems. The failing ridges should be propagating, while the propagating ridges should be failing. Clearly, other mechanisms in addition to the along-axis topographic gradients must be considered to derive a self-consistent model for the SEIR propagators.

3.4. Sensitivity of K_I Calculations

The choice of the crack tip location can significantly influence the relative contributions to the stress intensity factors of the driving and resisting topographic gradients. As shown in Figures 6 and 7, our choices for crack tip locations (Figures 4a and 4b) correspond to the change of slope at the head of the tip depression as seen in the bathymetric data. This choice results in a reference bathymetric datum that is close to the depth of surrounding, undisrupted seafloor (Table 1). It is worthwhile, however, to examine the sensitivity of the stress intensity factor to small relocations of the position

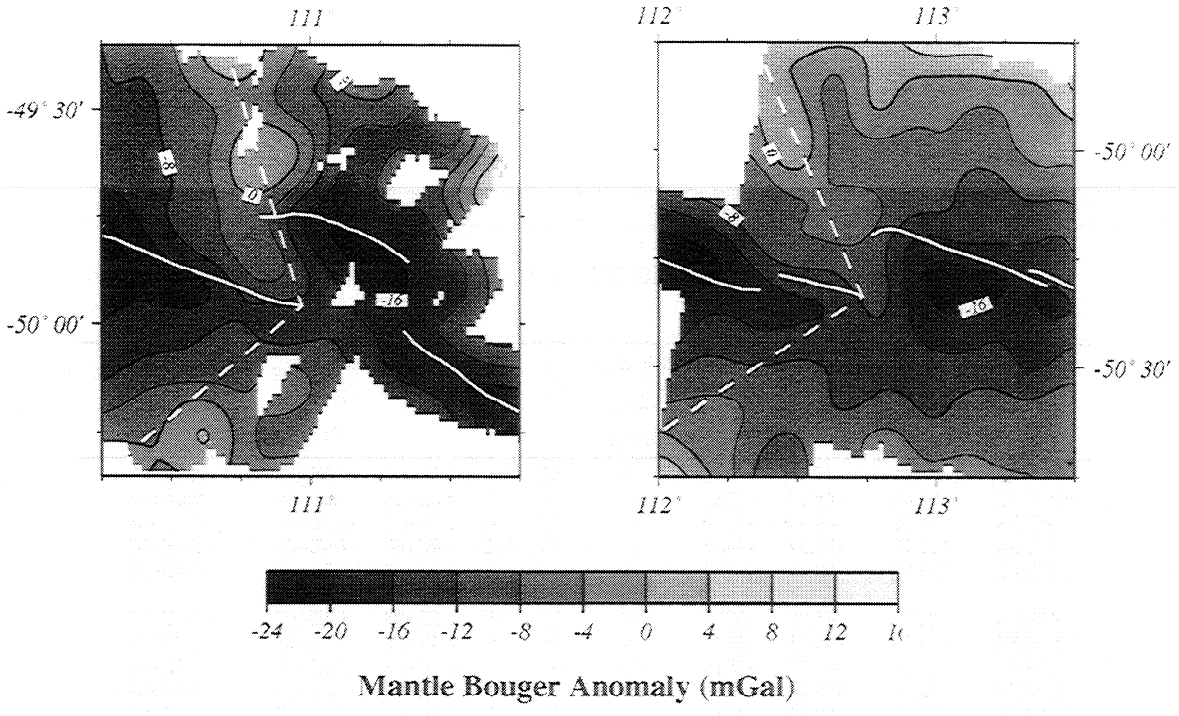

Figure 5. The mantle Bouguer gravity anomaly (MBA) for the 111°E and 113°E SEIR PRs. Solid lines trace the ridge axis; dashed lines denote the traces of the pseudofaults. Other SEIR propagators are not shown due to a lack of adequate gravity data coverage or are previously published (e.g., see *West and Sempéré* [1998]; note that this study also shows the 104°E PR as a region of locally thinned crust). The MBA was calculated using standard three-dimensional analysis of gravity anomaly data [*Parker*, 1973; *Prince and Forsyth*, 1988]. The gravity field due to seafloor topography and subsurface density variations was calculated from SeaBeam 2000 bathymetric data gridded using a minimum curvature algorithm [*Smith and Wessel*, 1990] with a spacing of 250 m. Density interfaces between seawater (1030 kg m^{-3}), crust (2730 kg m^{-3}), and mantle (3330 kg m^{-3}) were assumed to follow the seafloor topography with a crust-mantle boundary at a constant depth of 6 km [*Chen*, 1992] below the seafloor. The MBA values were obtained by point-by-point subtraction of the mantle Bouguer correction from the free-air gravity anomaly described by *Cochran et al.* [1997].

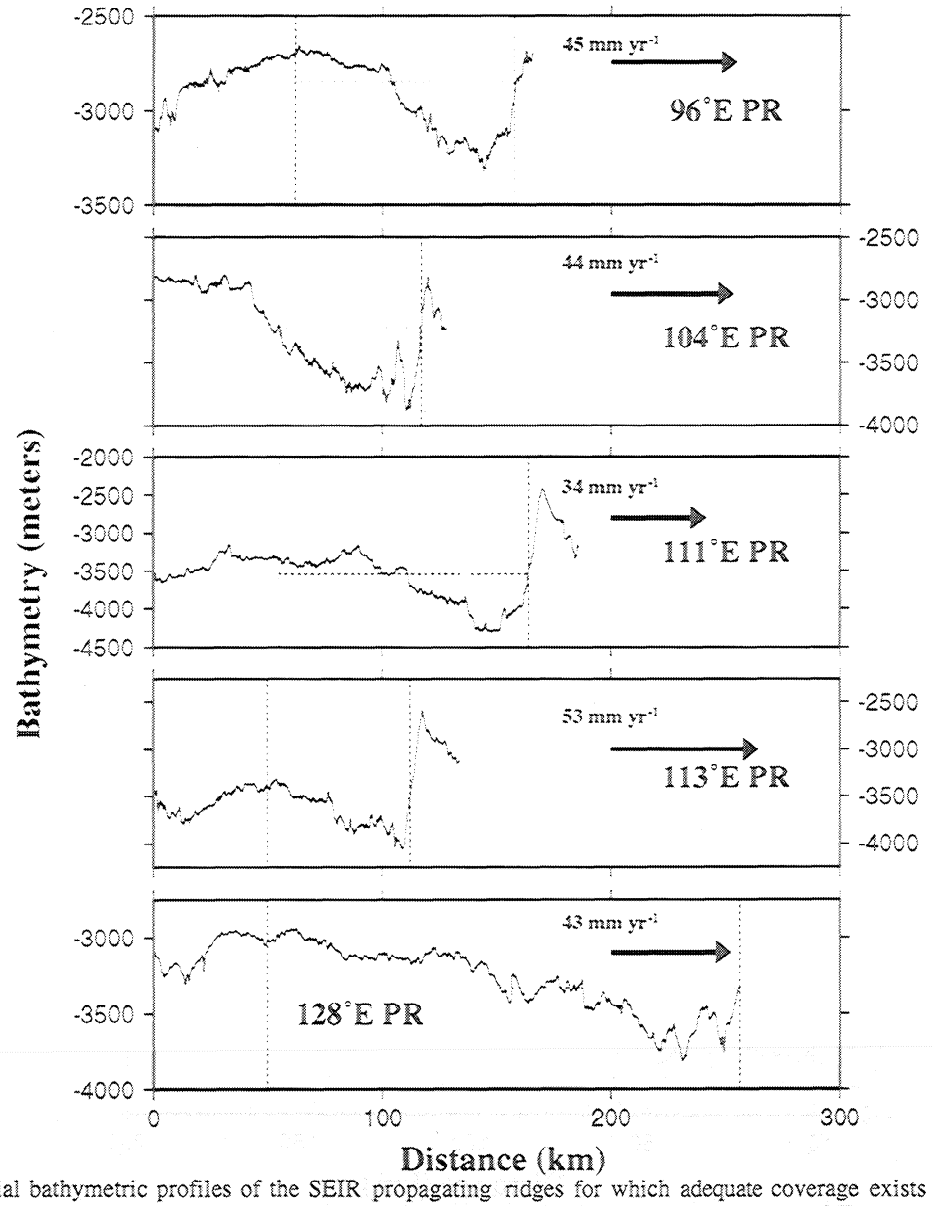

Figure 6. Axial bathymetric profiles of the SEIR propagating ridges for which adequate coverage exists on both the PR and FR. Left and right (dotted) vertical lines of each panel indicates the "A" and "B" distances of Table 1, respectively and correspond to 0 and L in the limits of integration for equation (2). The right vertical line indicates the location of crack tip, while the horizontal (dotted) line indicates the depth of the crack tip. Arrows and notation indicate the propagation velocity. Locations of the ridge axis profiles and propagating tips are geographically shown in Figures 4a and 4b. Significant tectonic unroofing and uplift ahead of the more magmatically starved propagating ridges can be observed in these profiles as the relatively shallow topography adjacent to the PRs.

of the propagator tip. If the propagating tip is chosen further from the segment center (toward shallower topography; Figures 6 and 7), the resisting force will increase because the reference bathymetric datum is decreased. If the propagating tip is chosen closer to the center of the segment (initially toward deeper topography; Figures 6 and 7), the resisting force will decrease. In both cases, however, the driving and resisting forces are relatively insensitive to changes in tip location owing to the r^{-2} relationship of (2).

4. Effects of Crustal Thickness and Asthenospheric Flow on Ridge Propagation

In order to remedy some of the problems discussed above, we modified the original fracture mechanics model of ridge propagation to include additional mechanisms that can affect the force balance and result in the consistent propagation of the SEIR PRs toward the AAD, despite significant variations in axial morphology and segmentation.

4.1. Contribution of Variable Crustal Thickness to K_I

If we assume that the near-axis elastic plate thickness H is less than the crustal thickness, the Pratt-type isostasy [*Turcotte and Schubert*, 1982] used by *Phipps Morgan and Parmentier* [1985] is not valid because density interfaces lie below the compensation depth, $\delta \div H$. This is likely the case for axial high morphologies, where the "decoupling zone" is wider than "the failure zone" [*Chen and Morgan*, 1990b]). In such cases, along-axis variations in crustal thickness may provide a significant fraction of the driving force for ridge propagation. In order to quantify this effect, we modify the description of the horizontal force per unit length (equation

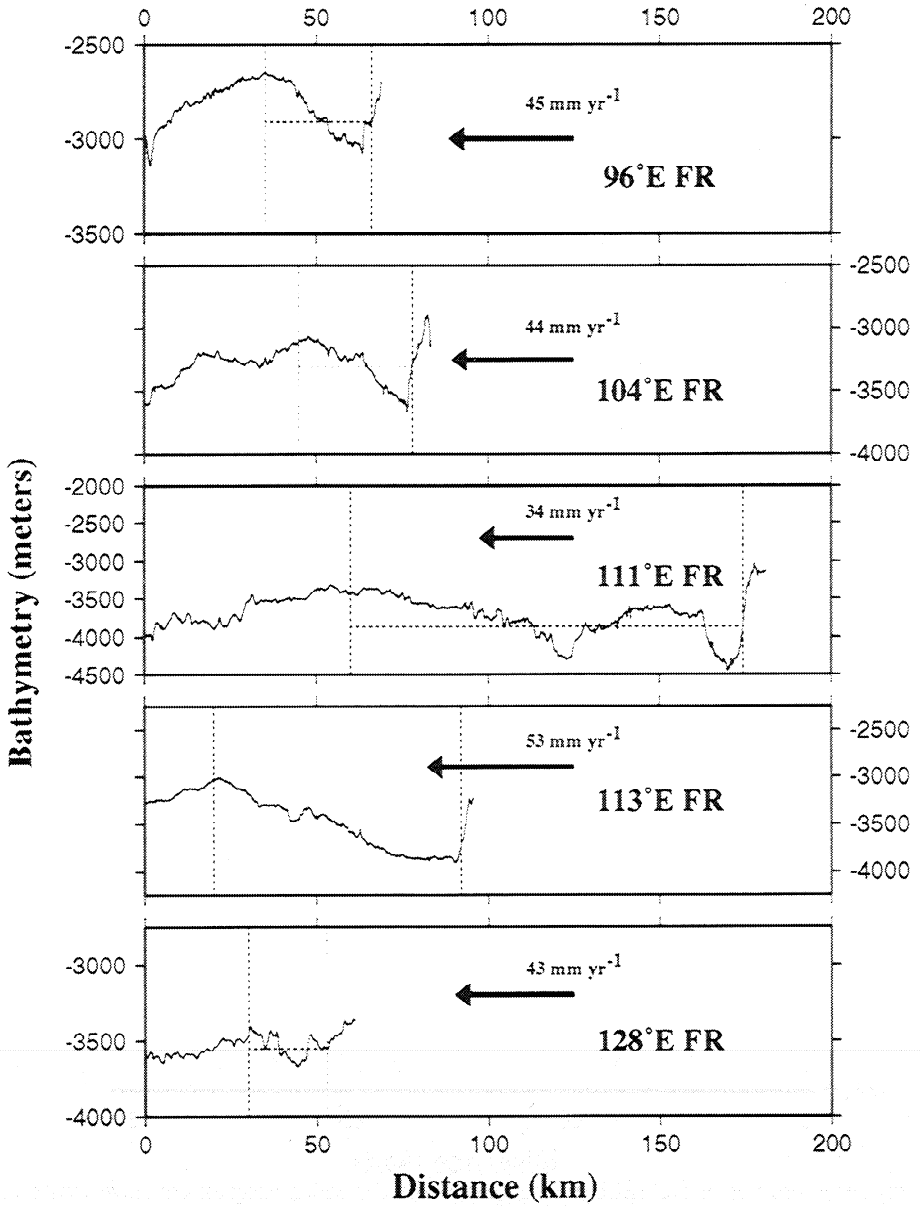

Figure 7. Axial bathymetric profiles of the SEIR failing ridges for which adequate coverage exists on both the PR and FR. See Figure 6 for further details. In the case of the FR the black vectors indicate the velocity with which the failing rift is retreating, which is equal to the propagation rate of the PR shown in Figure 6. Locations of the ridge axis profiles, and propagating tips are shown in Figures 4a and 4b.

(1)) to include a second density surface, an isostatically compensating crust-mantle interface, in addition to the seafloor [*Turcotte and Schubert*, 1982]:

$$P(x) = (\rho_c - \rho_w) g \delta H / 2 + \beta (\rho_m - \rho_c) g \frac{(\rho_c - \rho_w)}{(\rho_m - \rho_c)} \delta H / 2, \quad (3a)$$

where β is a factor describing the degree to which seafloor topography is compensated by the underlying Moho and δ is the depth of the propagating rift tip above which is the excess topography and below which is the isostatically compensating Moho. Other variables are as previously defined. For simplicity in our calculations we assume β=1.0, and thus zero-age seafloor is perfectly compensated by along-axis variations in crustal thickness in Airy mode:

$$P(x) = (\rho_c - \rho_w) g \delta H. \quad (3b)$$

Equations (3a) and (3b) can be thought of as expressions for the horizontal force per unit length of ridge axis due to excess topography that is supported by local Airy isostasy where the compensating density interface is the Moho. This scenario is shown schematically in Figure 9.

4.2. Contribution of Asthenospheric Flow to KI

Fundamental to this type of treatment is the assumption that for propagation to proceed, the forces driving ridge propagation and the forces resisting propagation must be in an appropriate dynamic equilibrium. If, for a given PR–FR pair, the driving forces calculated using (2) and (3b) do not exceed the resisting forces, a mechanism must be found that will provide the necessary additional driving force. At least for the SEIR, a probable additional source of driving force is subaxial asthenospheric flow. Regional-scale thermal modeling of the

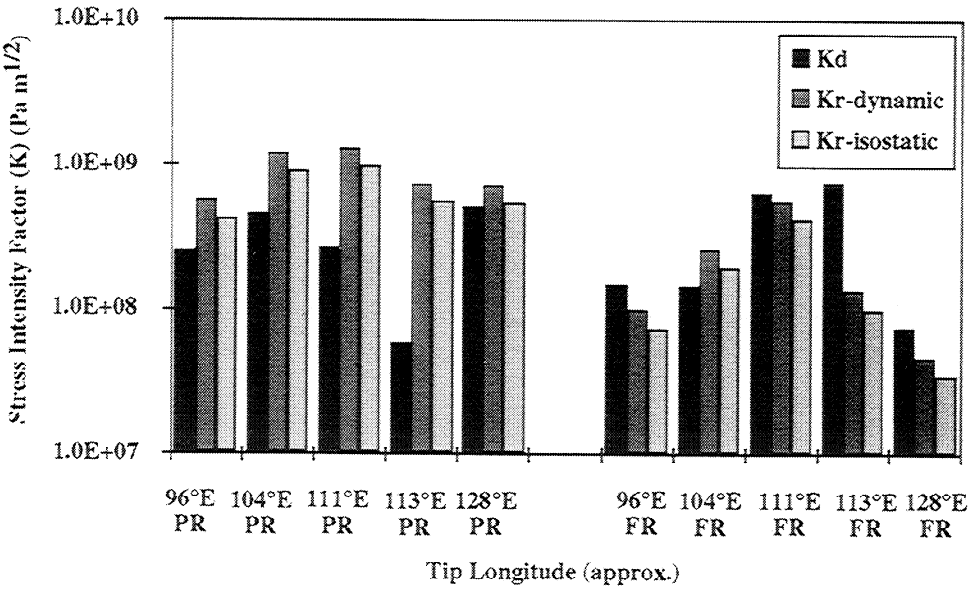

Figure 8. The driving (K_d) and resisting forces (K_r) for the PRs and FRs of the SEIR, according to the definitions of *Phipps Morgan and Parmentier* [1985]. For the actively propagating rifts (left-hand side), calculated resistive forces resulting from both dynamic and isostatic compensation exceed the calculated driving force. For actively failing rifts (right hand side), the driving force exceeds the resistive force (except for the 104°E FR, see text). According to these results the ridges that observed propagating should be failing, while those that are failing should be propagating. These force balances clearly demonstrate that factors other than those considered by the *Phipps Morgan and Parmentier* [1985] model must influence these PRs.

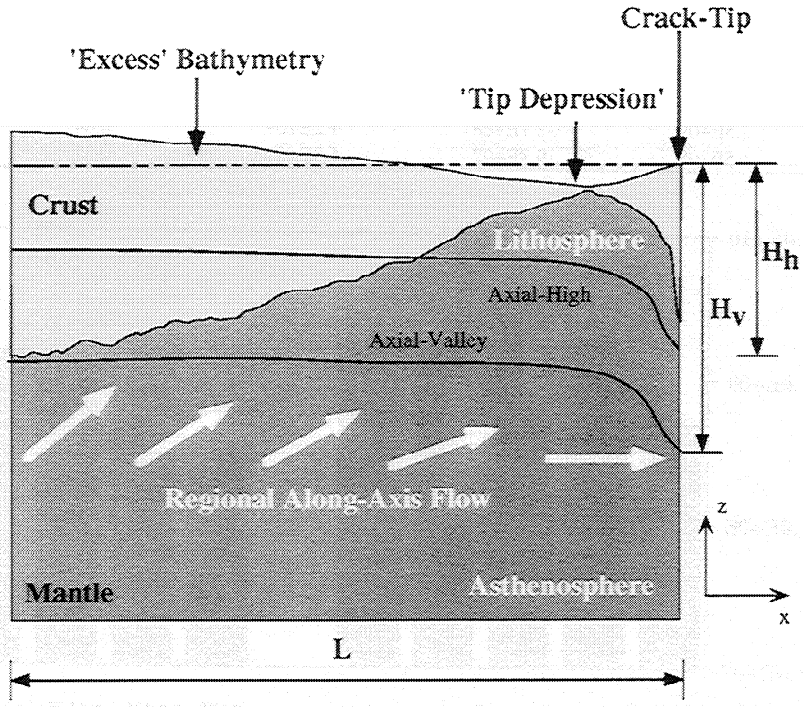

Figure 9. Schematic diagram of our new model for PRs driven by both excess, compensated bathymetry and regionally driven along-axis asthenospheric flow. Graphic definitions of the crack tip, tip depression, excess bathymetry, and crack length L are shown. In this model, topographic variation of the seafloor and of an isostatically compensating Moho contribute to the forces driving and resisting propagation. Solid black lines represent the depth of the lithosphere/asthenosphere transition for an axial high (H_h) and axial valley (H_v) scenario. In axial valley type morphology, the lack of a "decoupling zone" [*Chen and Morgan*, 1990a,b] would suggest that only the upper-mantle below a given thermal boundary layer would act as the asthenosphere and thus flow along-axis due to regional driving forces.

SEIR by *West et al.* [1997] showed that for a temperature-dependent, variable-viscosity mantle, regional mantle temperature gradients lead to axial depth and crustal thickness gradients and to subaxial asthenospheric flow. Earlier workers have also suggested that rift propagation may be driven by asthenospheric flow [e.g., *Vogt*, 1974; *Sempere et al.*, 1996; *West et al.*, 1997].

In order to quantify the additional effect of asthenospheric flow on the propagation driving force, we can treat any imbalance in the driving and resisting forces calculated by (3b) as a net imbalance in the stress intensity factor (K_I). As developed by *Phipps Morgan and Parmentier* [1985], the stress intensity factor resulting from the pressure variation associated with along-axis asthenospheric flow can be calculated by treating the pathway for flow as a half-infinite crack in the lithosphere, with the vertically integrated channel pressure applied on the crack surface. For a distribution of point forces $P(x)$ applied to both sides of the crack along a distance x from the crack tip [*Tada et al.*, 1973], the individual contribution to K_I is

$$\Delta \overline{K_I} = \left(\frac{2}{\pi x}\right)^{1/2} \frac{P(x)}{H}. \quad (4)$$

Phipps Morgan and Parmentier [1985] formulated the horizontal distribution of vertically integrated pressure as the superposition of infinitesimal point forces $P(x)dy$ and showed that the resulting stress intensity factor is

$$\overline{K_I} = \frac{32}{\pi^2}\left(\frac{H}{\pi}\right)^{3/2} Q \sum_{\text{odd } n} n^{-7/2} \quad (5)$$

where

$$Q = \frac{12\mu u_x}{d^2}, \quad (6)$$

and thus

$$\overline{K_I} = \frac{9\mu u_x H^{3/2}}{d^2}. \quad (7)$$

Table 2. Modified Driving and Resisting Forces and Estimated Along-Axis Asthenospheric Flows

Ridge	$K'_{driving}$, Pa $m^{1/2}$	$K'_{resisting}$, Pa $m^{1/2}$	$K'_d+K'_r$, Pa $m^{1/2}$	Differential Flow Rate, mm yr^{-1}	Asthenospheric Flow Rate, mm yr^{-1}
96°E PR	5.0E+08	-1.1E+09	-6.2E+08	-3.46	48.46
104°E PR	9.2E+08	-2.4E+09	-1.5E+09	-8.15	52.15
111°E PR	5.3E+08	-2.6E+09	-2.0E+09	-11.36	45.36
113°E PR	1.2E+08	-1.5E+09	-1.4E+09	-7.60	60.60
128°E PR	1.0E+09	-1.4E+09	-4.1E+08	-2.29	45.29
96°E FR	3.0E+08	-2.0E+08	1.0E+08	0.56	-45.56
104°E FR	2.9E+08	-5.2E+08	-2.3E+08	-1.29	-42.71
111°E FR	1.3E+09	-1.1E+09	1.5E+08	0.83	-34.83
113°E FR	1.5E+09	-2.7E+08	1.2E+09	6.84	-59.84
128°E FR	1.5E+08	-9.3E+07	5.8E+07	0.32	-43.32

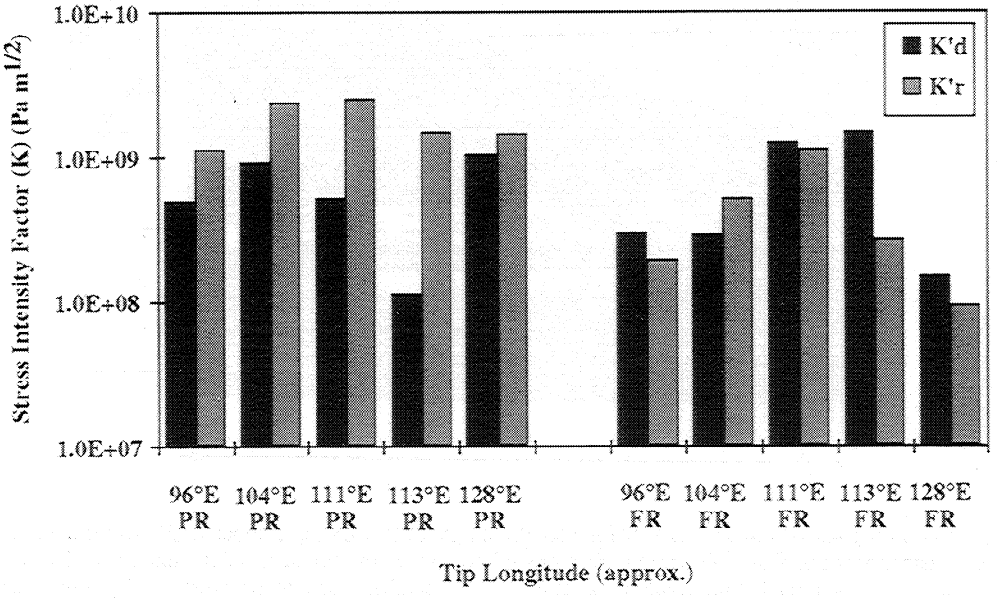

Figure 10. The driving (K'_d) and resisting (K'_r) forces for the PRs and FRs of the SEIR, according to our definitions of the horizontal force per unit length in (3). Again, in all cases for PRs the resisting forces are greater than the driving forces. FRs show the same characteristics as in Figure 8 with the driving forces usually exceeding the resisting forces. Again, the 104° FR is an exception to this trend, likely due to a recent ridge axis jump from the north.

In these relationships, μ is the viscosity of the asthenospheric channel, and u_x is the along-axis flow velocity in excess of the rift propagation speed. Further, H and d are the assumed depth and width of an asthenospheric flow "channel," respectively. Thus the excess asthenospheric flow velocity required to reach equilibrium at the propagator tip is given by

$$u_x = \frac{\overline{K_I} d^2}{9\mu H^{3/2}} = \frac{\left(K'_r - K'_d\right) d^2}{9\mu H^{3/2}}. \qquad (8)$$

A couple of points are now worth noting. First, in our derivation, the along-axis flow u_x is the intersegment along-axis flow that is driven by regional temperature gradients and not the along-axis, intra-segment, viscous resistance flow described by *Phipps Morgan and Parmentier* [1985]. Second, in this context, ridge propagation driven by asthenospheric flow is analogous to magmatically driven crack propagation, as described by *Spence and Turcotte* [1985]. Here we formulate the propagating rift as a crack in an elastic medium where the viscous resistance to flow in the crack is negligible compared to the fracture resistance of the medium. Thus (2), when vertically integrated, and equation (36) of *Spence and Turcotte* [1985], when integrated along the axis of the crack, are essentially the same. They differ only by a factor of $2\pi^{-1}$ since we have treated our crack as a "penny-shaped" crack, which is enclosed by the overlying lithosphere and open to the pressure field of the underlying asthenosphere (see Figure 6b of *Pollard*, [1989], for a definition of a penny-shaped crack). Our (2) and *Pollard and Aydin's* [1984] (4a) are identical when integrated vertically and along-axis.

4.3. Dynamics and Rate-Limiting Mechanisms of Flow-Driven Propagation

In order to maintain a long-term dynamic equilibrium, the propagation rate, averaged over time, must be equal to or less than the along-axis asthenospheric flow velocity. Instantaneously, however, the propagation rate can be faster than the along-axis flow velocity because tectonic fractures within the lithosphere can act on a shorter timescale than asthenospheric flow. Thus along-axis asthenospheric flow, while serving in as a long-term driving force for ridge propagation, will also act, on a shorter timescale, as a resisting force when tectonic stresses cause rapid advancement of the rift tip. The long-term along-axis component of mantle flow can be faster than the propagation rate if tectonic stresses hinder advancement of the lithospheric crack. An ideal situation (i.e., propagation through a uniform plate without complexities) is reached when the propagation rate through the lithosphere is equal to the asthenospheric flow rate.

For spreading centers with axial-high morphology, it has been proposed that lower crustal material may be "decoupled" from the rigid lithosphere (Figure 9) [*Chen and Morgan*, 1990a,b; *Shaw and Lin*, 1996], thus allowing the weak lower crust to flow with the deforming mantle (crustal material below H_h in Figure 9). For spreading centers with axial valley morphology, however, it is more likely that the lithosphere extends through the entire crustal section into the mantle so that only mantle material constitutes the flowing asthenosphere (mantle material below H_v in Figure 9). Thus the propagation velocity described by (8) could simplistically represent some complex combination of lower crustal and upper mantle along-axis flow velocities (and viscosities) in a region displaying an axial high.

4.4. Estimates of the SEIR Asthenospheric Flow Velocities

Table 2 and Figure 10 show the results of our analysis of the SEIR propagating and failing ridges using the more complex formulations that we have derived. First, when we apply (2) and (3) using the same tip locations as before (Table 1), we find similar results (Table 2 and Figure 10) as when we applied the *Phipps Morgan and Parmentier* [1985] formula. The observed propagation is not predicted for any SEIR PR/FR pair: resisting forces are greater than driving forces for all PRs, while driving forces exceed resisting forces for all FRs (with the exception of the 104° E FR, as discussed above; Figure 4a). This demonstrates that topographic variability is not sufficient to explain the observed propagation. iiiiiiiiikBy calculating the along-axis flow magnitudes required to balance forces and drive ridge propagation for each SEIR PR/FR pair in turn, we evaluate our hypothesis for consistency. The results show that for reasonable flow magnitudes this mechanism can reproduce the observed propagation, consistent in rate and direction, despite widely varying axial depths (Figure 11). In the calculation the extra flow (Table 2) is superimposed on the observed propagation velocity (Table 1) and calculated assuming d=H=25 km and μ=10^{19} Pa s. For these choices of d, H, and μ the calculated along-axis flow values are consistent with estimates of the along-axis flow velocities beneath the SEIR based on regional-scale mantle convection models [*West et al.*, 1997]. The estimated flow magnitude for the 113°E system is greater than that estimated for the other locations. This may reflect the first-order nature of the calculations, indicating the extent to which d, H, and μ may vary along the SEIR, or it may represent a local perturbation, such as the superposition of a three-dimensional, segment-scale mantle upwelling structure.

A second point of consistency is that PR/FR pairs with similar offsets appear to have similar along-axis flow velocities (e.g., 96°E, 113°E, and 128°E). This can be explained as follows. For small-offset propagators the two segments sample the same part of the along-axis flow field. For increasingly large offsets the likelihood of sampling different local velocities within a continuously varying flow field increases until, for sufficiently large offsets (e.g., 111°E) or recent ridge jumps (e.g., 104°E), the offset itself may perturb the subaxial flow field, thereby enhancing or creating the intersegment flow velocity contrasts.

5. Discussion

Our calculations demonstrate that at least in the case of the Southeast Indian Ridge (SEIR), along-axis asthenospheric flow is likely a first-order driving force for ridge propagation and that modifications are required to simpler models for the driving forces of ridge propagation based primarily on the Galápagos and Easter propagating rifts. In the light of our more complex model, we can now reexamine some of the earlier data.

5.1. Galápagos 95.5°W Propagating Rift

Using (1) and (2), *Phipps Morgan and Parmentier* [1985] showed that the driving (K_d) and resisting (K_r) forces of the Galápagos (95.5°W) PR are approximately balanced with the driving and resisting stress intensity factors at the crack tip equaling 4 x 10^9 Pa $m^{1/2}$ and –4 x 10^9 Pa $m^{1/2}$, respectively. When we incorporate the topographic gradient of the Moho

into the calculation, these values become 8 x 10^{-9} Pa $m^{1/2}$ and -8 x 10^{9} Pa $m^{1/2}$ (equation (3)). Here, we assume an isostatically compensated topographic gradient, consistent with recent findings of *Ito and Lin* [1995] and *Ito et al.* [1997], who showed that ~70-80% percent of the long-wavelength variations in crustal thickness on the Cocos-Nazca Ridge can be explained by crustal thickness variations. We conclude that the along-axis asthenospheric flow beneath the Galápagos (95.5°W) propagator is approximately equal to the known propagation rate (53 mm yr^{-1}) since no extra asthenospheric "push" is required to balance driving and resisting forces. Thus this PR is in equilibrium with the underlying along-axis asthenospheric flow. A similar conclusion can be reached for the Easter PRs.

5.2. Axial Morphologic Variations Along Propagating Ridge Segments

A common characteristic of all observed PRs is that the "tip depression," an axial region that is deeper and more deficient in magma supply than the remainder of the propagating segment. For example, the magmatically robust Galápagos 95.5°W propagating ridge is characterized by an axial high away from the axial valley at the propagating tip. At the other end of the spectrum the shallow axial valley of the magmatically starved SEIR, 113° E PR deepens and widens into the tip (Figure 4a).

Small variations in crustal thickness may significantly modify the overall strength of near-axis lithosphere and thereby influence how it deforms in response to extensional and buoyant forces. Several recent theoretical studies have addressed the relationship between axial topography and crustal thickness [*Chen and Morgan*, 1990a,b; *Shaw and Lin*, 1996]. *Chen and Morgan* [1990a,b], for example, proposed that the axial topography of mid-ocean ridges is the result of the relative width of a "decoupling zone" beneath the ridge where stresses in the brittle plate due to mantle flow exceed the yield strength. The cross-axis width of this decoupling zone is primarily a function of the thickness of the oceanic crust and its thermal structure. At slow spreading ridges or in regions with thin crust, coupling between ridge-perpendicular mantle flow and the crust will result in deformation of the elastic plate and the formation of a rift valley. In contrast, at faster spreading ridges or in regions of thicker crust, where the elastic plate is relatively weak and prone to break along-axis, the greater width of the decoupling zone will cause the mantle and the plate to respond separately to extension. Buoyancy forces may then lead to uplift of the broken plate and the creation of an axial high [*Chen and Morgan*, 1990a,b; *Magde and Detrick*, 1995].

Ridge propagation creates unique thermal and mechanical environments at the propagating tip, where older and substantially thicker lithosphere bounds the active rift tip. Regardless of spreading rate or axial topography, these conditions will inhibit the development of a decoupling zone beneath the advancing rift, promoting the development of the axial valley structure known as the tip depression. Thus the rift valley at a propagator tip is a consequence of rifting in the cooler thermal regime of preexisting lithosphere, rather than a consequence of viscous resistance flow as previously suggested [*Phipps Morgan and Parmentier*, 1985].

5.3. Geochemical Implications of Flow-Driven Ridge Propagation

Wilson and Hey [1995] interpreted patterns of high magnetization around the Galápagos hotspot to reflect the eruption of fractionated lavas in response to gradients in

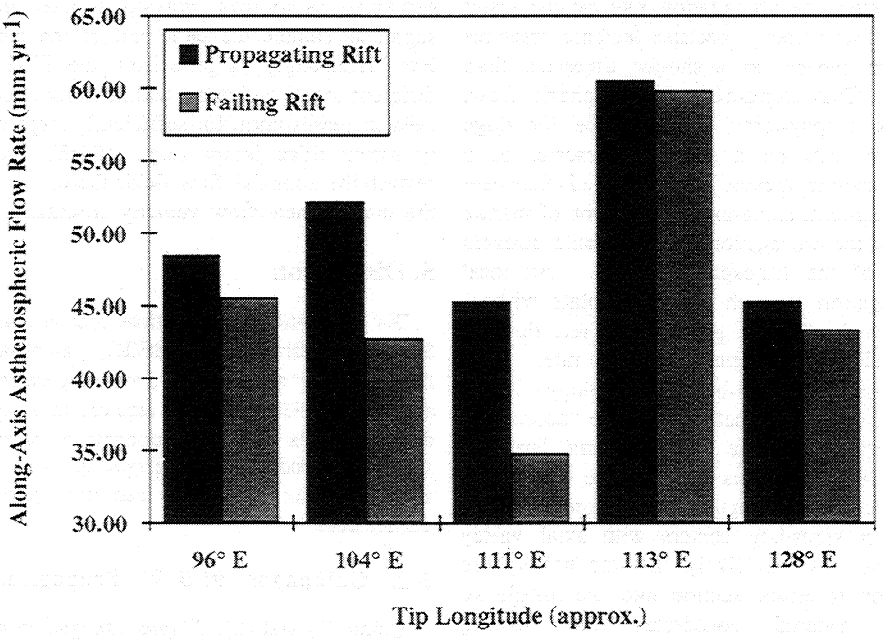

Figure 11. Predicted along-axis asthenospheric flow rates for the SEIR PRs and FRs (defined as positive if motion is toward the center of the AAD near ~120°E). These values were calculated using d=H=25 km and μ=10^{19} Pa s and the observed (long-term averaged) propagation rate. Since the dimensions of any asthenospheric channel are likely highly variable along the SEIR, these calculations are performed only as first-order estimates of the asthenospheric flow velocity.

magma supply and along-axis flow of hotspot-derived asthenosphere. According to this interpretation, eruptions at the distal end of a segment with a strong gradient in magma supply (such as a propagating rift tip) will be dominated by evolved magmas arriving from the segment center rather than by primitive magmas extracted from the mantle below.

Alternatively, *Christie and Sinton* [1981] argued that the extensive fractionation of lavas from the 95.5°W propagator in the Galápagos can be explained by the unique thermal gradient near the propagating tip and that the extent of differentiation is controlled by a balance between cooling rate and magma supply rate. Before a mature magma system is established behind the propagating ridge tip, isolated magma pools some distance behind the PR tip are cooled at optimal rates, leading to extensive fractionation. At the PR tip, differentiation is impeded by rapid cooling, and primitive lavas can only erupt in direct response to tectonic disruptions. These findings were later extended to the 85°W Galápagos and Juan de Fuca PRs by *Sinton et al.* [1983], who also showed that the strongest geochemical (and, by implication, magnetic) anomalies develop when the propagation direction is parallel to the absolute motion of the plate boundary.

Along the SEIR, however, the chemical anomalies associated with the PRs are relatively weak, extending over relatively short distances and encompassing relatively small ranges of FeO and other differentiation indicators (*B. Sylvander et al.*, manuscript in preparation, 1997). This apparent suppression of the PR-related magmatic perturbation may partly reflect the northward absolute motion of the SEIR, orthogonal to the propagation directions, but it may also result from the involvement of along-axis asthenospheric flow in the propagation process, as we have described. Along-axis mantle flow, moving in the same direction as propagation, will effectively reduce the differential motion of the rift tip relative to the asthenosphere, shortening the distance over which enhanced fractionation exists.

Other potentially important factors affecting the thermal balance at a propagating rift tip include, specific mantle temperature and ridge offset geometry, both of which may influence the thickness of the lithosphere into which the rift is propagating. For example, for a given offset length a warmer asthenosphere will cause a steeper along-axis temperature gradient, and the fractionation peak will be closer to the rift tip. For the same reasons, at a given upper mantle temperature, larger offset between the PR and FR will cause the thermal structure of the tip to be colder, the along-axis temperature gradient to be greater, and the fractionation peak to be farther from the rift tip. Evaluation of these additional effects would require additional data beyond the scope of this study.

6. Conclusions

1. Regardless of specific compensation styles, models for rift propagation that incorporate only topographically derived forces are unable to explain the continuous propagation, at uniform velocity, of Southeast Indian Ridge PRs over a range of axial depths and morphologies. Progressively more complex numerical treatments show that a non isostatic mechanism, most likely down axis, regional asthenospheric flow, is required for a more self-consistent rift propagation model in this region. Along-axis flow within an asthenospheric channel beneath a ridge segment can provide a positive contribution to the stress intensity factor, promoting propagation at a uniform rate and in a consistent direction, despite diverse axial morphologic signatures, non monotonic axial bathymetry gradients, and variable segmentation characteristics.

2. The presence of an axial valley at the propagating rift tip reflects lithospheric thinning and reduced magma supply as a natural consequence of rifting into the cooler thermal regime of preexisting lithosphere. The thinning of oceanic crust near the propagating tips of the SEIR is consistent with the evolution patterns of magmatism behind the advancing tip [*Christie and Sinton*, 1981; *Sinton et al.*, 1983] and with theoretical models of lithospheric stretching as a mechanism for formation of axial valleys at spreading centers [e.g., *Tapponier and Francheteau*, 1978; *Chen and Morgan*, 1990a,b; *Neumann and Forsyth*, 1993; *Phipps Morgan and Chen*, 1993; *Shaw and Lin*, 1996].

Acknowledgments. Contributions to this study by B. Sylvander, J.-C. Sempéré, J. Cochran, and C. Small are gratefully acknowledged. We thank the many who contributed to the quality bathymetry data presented in this study. We also thank J. Dañobeita for use of the newly acquired axial bathymetry data from the Cocos-Nazca spreading center. Comments and suggestions by A. Hosford, R. Detrick, H. Schouten, B. Tucholke, D. Wilson, Y.-J. Chen, and an anynonymous reviewer significantly improved the quality of this work. This study was supported by a Woods Hole Oceanographic Institution Post-Doctoral Fellowship to B.P.W., and is contribution 9663 of the Woods Hole Oceanographic Institution. Support under the following National Science Foundation grants is gratefully acknowledged: OCE-9520521, OCE-9400395 (to Christie), and OCE-9420694 (to J.-C. Sempéré), and OCE-9811924 (to Lin).

References

Brozena, J.M., and R.S. White, Ridge jumps and propagations in the South Atlantic Ocean, *Nature*, *348*, 149-152, 1990.

Carbotte, S.M., S.M. Welch, and K.C. Macdonald, Spreading rates, rift propagation and fracture zone offset histories during the past 5 my on the Mid-Atlantic Ridge: 25°-27°30'S and 31°-34°30'S, *Mar. Geophys. Res.*, *13*, 51-80, 1991.

Chen, Y.J., Oceanic crustal thickness versus spreading rate, *Geophys. Res. Lett.*, *19*, 753-756, 1992.

Chen, Y.J., and W.J. Morgan, A nonlinear rheology model for mid-ocean ridge axis topography, *J. Geophys. Res.*, *95*, 17583-17604, 1990a.

Chen, Y.J., and W.J. Morgan, Rift valley/no rift valley transition at mid-ocean ridges, *J. Geophys. Res.*, *95*, 17571-17581, 1990b.

Christie, D.M., and J.M. Sinton, Evolution of abyssal lavas along propagating segments of the Galápagos spreading center, *Earth Planet. Sci. Lett.*, *56*, 321-355, 1981.

Christie, D.M., and J.M. Sinton, Major element constraints on melting, differentiation and mixing of magmas from the Galápagos 95.5°W propagating rift system, *Contrib. Mineral. Petrol.*, *94*, 274-288, 1986.

Cochran, J.R., J.-C. Sempéré, and SEIR Scientific Team, The Southeast Indian Ridge between 88°E and 118°E: Gravity anomalies and crustal accretion at intermediate spreading rates, *J. Geophys. Res.*, *102*, 15463-15487, 1997.

Géli, L., et al., The evolution of the Pacific-Antarctic Ridge south of the Udintsev Fracture Zone, *Science*, *278*, 1281-1284, 1997.

Grindlay, N.R., J. Madsen, C. Rommevaux, J. Sclater, and S. Murphy, Southwest Indian Ridge 15°E-35°E: A geophysical investigation of an ultra-slow spreading mid-ocean ridge system, *InterRidge News*, *5*, 7-12, 1996.

Hey, R., and P.R. Vogt, Spreading center jumps and sub-axial asthenosphere flow near the Galápagos hotspot, *Tectonophysics*, *37*, 41-52, 1977.

Ito, G., and J. Lin, Mantle temperature anomalies along the present and paleoaxes of the Galápagos spreading center as inferred from gravity analyses, *J. Geophys. Res.*, *100*, 3733-3745, 1995.

Ito, G., J. Lin, and C.W. Gable, Interaction of mantle plumes and

migrating midocean ridges: Implications for the Galápagos plume-ridge system, *J. Geophys. Res.*, *102*, 15403-15417, 1997.

Kleinrock, M.C., and R.N. Hey, Detailed tectonics near the tip of the Galapaos 95.5°W propagator: How the lithosphere tears and a spreading axis develops, *J. Geophys. Res.*, *94*, 13801-13838, 1989a.

Kleinrock, M.C., and R.N. Hey, Migrating transform zone and lithospheric transfer at the Galápagos 95.5°W propagator, *J. Geophys Res.*, *94*, 13859-13878, 1989b.

Kleinrock, M.C., R.C. Searle, and R.N. Hey, Tectonics of the failing spreading system associated with the 95.5° W Galápagos propagator, *J. Geophys. Res*, *94*, 13839-13857, 1989.

Livermore, R., A. Cunningham, L. Vanneste, and R. Larter, Subduction influence on magma supply at the East Scotia Ridge, *Earth Planet. Sci. Lett.*, *150*, 261-275, 1997.

Macdonald, K.C., and P.J. Fox, Overlapping spreading centers: New accretion geometry on the East Pacific Rise, *Nature*, *302*, 55-58, 1983.

Macdonald, K., J.-C. Sempere, and P.J. Fox, East Pacific Rise from Siqueiros to Orozco fracture zones: Along-strike continuity of axial neovolcanic zone and structure and evolution of overlapping spreading centers, *J. Geophys. Res.*, *89*, 6049-6069, 1984.

Magde, L.S., and R.S. Detrick, Crustal and upper mantle contribution to the axial gravity anomaly of the southern East Pacific Rise, *J. Geophys. Res.*, *100*, 3747-3766, 1995.

Neumann, G.A., and D.W. Forsyth, The paradox of the axial profile: Isostatic compensation along the axis of the Mid-Atlantic Ridge?, *J. Geophys. Res.*, *98*, 17891-17910, 1993.

Palmer, J., J.-C. Sempéré, D.M. Christie, and J.P. Morgan, Morphology and tectonics of the Australian-Antarctic Discordance between 123°E and 128°E, *Mar. Geophys. Res.*, *15*, 121-152, 1993.

Parker, A.P., *The Mechanics of Fracture and Fatigue*, F. N. Spon, New York, 1981.

Parker, R.L., The rapid calculation of potential anomalies, *Geophys. J. R. Astron. Soc.*, *31*, 447-455, 1973.

Parmentier, E.M., and D.W. Forsyth, Three-dimensional flow beneath a slow spreading ridge axis: A dynamic contribution to the deepening of the median valley toward fracture zones, *J. Geophys. Res.*, *90*, 678-684, 1985.

Perram, L.J., et al., Magnetic and tectonic studies of the dueling propagating spreading centers at 20°40' S on the East Pacific Rise: Evidence for crustal rotations, *J. Geophys. Res.*, *98*, 13835-13850, 1993.

Phipps Morgan, J., and Y.J. Chen, The genesis of oceanic crust: Magma injection, hydrothermal circulation and crustal flow, *J. Geophys. Res.*, *98*, 6283-6297, 1993.

Phipps Morgan, J., and M.C. Kleinrock, Transform zone migration: Implications of bookshelf faulting at oceanic and Icelandic propagating ridges, *Tectonics*, *10*, 920-935, 1991.

Phipps Morgan, J., and E.M. Parmentier, Causes and rate-limiting mechanisms of ridge propagation: A fracture mechanics model, *J. Geophys. Res.*, *90*, 8603-8612, 1985.

Phipps Morgan, J., and E.M. Parmentier, A three-dimensional gravity study of the 95.5°W propagating rift in the Galápagos spreading center, *Earth Planet. Sci. Lett.*, *81*, 289-298, 1986.

Phipps Morgan, J., and D.T. Sandwell, Systematics of ridge propagation south of 30° S, *Earth Planet. Sci. Lett.*, *121*, 245-258, 1994.

Pollard, D.D., Elementary fracture mechanics applied to the structural interpretation of dykes, in *Mafic Dyke Swarms*, edited by J.C. Halls and W.F. Fahrig, *Geol. Assoc. Can. Spec. Pap.*, *34*, 5-24, 1989.

Pollard, D.D., and A. Aydin, Propagation and linkage of oceanic ridge segments, J. Geophys. Res., 89, 10017-10028, 1984.

Prince, R.A., and D.W. Forsyth, Horizontal extent of anomalously thick crust near the Vema Fracture Zone from the three-dimensional analysis of gravity anomalies, *J. Geophys. Res.*, *93*, 8051-8063, 1988.

Scheirer, D., M. Eberle, and D. Forsyth, The influence of the Amsterdam-St. Paul Hotspot on the morphology of the Southeast Indian Ridge, *Eos Trans. AGU*, *78*(46), Fall Meet. Suppl., F674, 1997.

Searle, R.S., and R.N. Hey, GLORIA observations of the propagating rift at 95.5°W on the Cocos-Nazca spreading center, *J. Geophys. Res.*, *88*, 6433-6447, 1983.

Sempéré, J.-C., and K. Macdonald, Overlapping spreading centers: implication from crack growth simulation by the displacement discontinuity method, *Tectonics*, *5*, 151-163, 1986.

Sempéré, J.-C., B.P. West, and L. Géli, The Southeast Indian Ridge between 127° and 132°40'E: Contrasts in segmentation characteristics and implications for crustal accretion, in *Tectonic, Magmatic, Hydrothermal and Biological Segmentation of Mid-Ocean Ridges*, edited by C.J. MacLeaod, P.A. Tyler, and C.A. Walker, pp. 1-15, Geol. Soc., London, 1996.

Sempéré, J.-C., J.R. Cochran, and others, The Southeast Indian Ridge between 88° and 118°: Variations in crustal accretion at a constant spreading rate, *J. Geophys. Res.*, *102*, 15489-15505, 1997.

Shah, A., and J.-C. Sempéré, Morphology of the transition from an axial high to an axial valley at the Southeast Indian Ridge and the relation to variations in mantle temperature, *J. Geophys. Res.*, *103*, 5203-5223, 1997.

Shaw, W.J., and J. Lin, Models of ocean ridge lithospheric deformation: Dependence on crustal thickness, spreading rate, and segmentation, *J. Geophys. Res.*, *101*, 17977-17993, 1996.

Shih, J., and P. Molnar, Analysis and implications of the sequence of ridge jumps that eliminated the Surveyer Transform fault, *J. Geophys. Res.*, *80*, 4815-4822, 1975.

Shoberg, T., et al., Constraints on rift propagation history at the Cobb offset, Juan de Fuca Ridge, from numerical modelling of tectonic fabric, *Tectonophysics*, *197*, 295-308, 1991.

Sinton, J.M., D.S. Wilson, D.M. Christie, R.N. Hey, and J.R. Delaney, Petrologic consequences of rift propagation on oceanic spreading ridges, *Earth Planet. Sci. Lett.*, *62*, 193-207, 1983.

Smith, W.H.F., and P. Wessel, Gridding with continuous splines in tension, *Geophysics*, *55*, 293-305, 1990.

Spence, D.A., and D.L. Turcotte, Magma-driven propagation of cracks, *J. Geophys. Res.*, *90*, 575-580, 1985.

Tada, H., P.C. Paris, and G.R. Irwin, *The Stress Analysis of Cracks Handbook*, Del Research Corporation, Hellertown, Penn., 1973.

Tapponnier, P., and J. Francheteau, Necking of the lithosphere and the mechanics of slowly accreting plate boundaries, *J. Geophys. Res.*, *83*, 3955-3970, 1978.

Turcotte, D.L., and G. Schubert, *Geodynamics: Applications of Continuum Physics to Geological Problems*, 450 pp., John Wiley, New York, 1982.

Vogt, P.R., Asthenospheric motion recorded by the ocean floor south of Iceland, *Earth Planet. Sci. Lett.*, *13*, 155-160, 1971.

Vogt, P.R., The Iceland phenomenon: Imprints of a hot spot on the ocean crust, and implications for flow below the plates, in *Geodynamics of Iceland and the north Atlantic area*, edited by L. Kristjansson, pp. 105-126, D. Reidel, Norwell, Mass., 1974.

West, B.P., and J.-C. Sempéré, Gravity anomalies, flexure of axial lithosphere, and along-axis asthenospheric flow beneath the Southeast Indian Ridge, *Earth Planet. Sci. Letter*, *156*, 253-266, 1998.

West, B.P., J.-C. Sempéré, D.G. Pyle, J. Phipps Morgan, and D.M. Christie, Evidence for variable upper mantle temperature and crustal thickness in and near the Australian-Antarctic Discordance, *Earth Planet Sci. Lett.*, *128*, 135-153, 1994.

West, B.P., W.S.D. Wilcock, J.-C. Sempéré, and L. Géli, Three-dimensional structure of asthenospheric flow beneath the Southeast Indian Ridge, *J. Geophys. Res.*, *102*, 7783-7802, 1997.

Wilson, D.S., Kinematics of overlapping rift propagation with cyclic rift failure, *Earth Planet. Sci. Lett.*, *96*, 384-392, 1990.

Wilson, D.S., and R.N. Hey, History of rift propagation and magnetization intensity for the Cocos-Nazca spreading center, *J. Geophys. Res.*, *100*, 10041-10056, 1995.

Wilson, D.S., R.N. Hey, and C. Nishimura, Propagation as a mechanism of reorientation of the Juan de Fuca Ridge, *J. Geophys. Res.*, *89*, 9215-9227, 1984.

D. M. Christie, College of Oceanic and Atmospheric Sciences, Oregon State University, Corvallis, OR 97331. (dchristie@oce.orst.edu)

J. Lin, Department of Geology and Geophysics, Woods Hole Oceanographic Institution, Woods Hole, MA 02543.

B. P. West, Exxon Production Research Company, P.O. Box 2189, Houston, TX 77252-2189.

(Received March 19, 1998; revised April 8, 1999;
accepted April 20, 1999.)